



Human Dopamine Transporter: The first implementation of a combined in silico/in vitro approach revealing the substrate and inhibitor specificities

Teodora Djikic, Yasmina Martí, Francesca Spyraakis, Thorsten Lau, Paolo Benedetti, Gavin Davey, Patrick Schloss & Kemal Yelekci

To cite this article: Teodora Djikic, Yasmina Martí, Francesca Spyraakis, Thorsten Lau, Paolo Benedetti, Gavin Davey, Patrick Schloss & Kemal Yelekci (2018): Human Dopamine Transporter: The first implementation of a combined in silico/in vitro approach revealing the substrate and inhibitor specificities, Journal of Biomolecular Structure and Dynamics, DOI: [10.1080/07391102.2018.1426044](https://doi.org/10.1080/07391102.2018.1426044)

To link to this article: <https://doi.org/10.1080/07391102.2018.1426044>



Accepted author version posted online: 15 Jan 2018.



Submit your article to this journal [↗](#)



View related articles [↗](#)



View Crossmark data [↗](#)

Publisher: Taylor & Francis

Journal: *Journal of Biomolecular Structure and Dynamics*

DOI: <http://doi.org/10.1080/07391102.2018.1426044>



Human Dopamine Transporter: The first implementation of a combined *in silico/in vitro* approach revealing the substrate and inhibitor specificities

Teodora Djikic ^{a,++}, Yasmina Marti ^{b,f,+}, Francesca Spyrakis ^{c,+}, Thorsten Lau ^{b,+}, Paolo Benedetti ^d, Gavin Davey ^e, Patrick Schloss ^f and Kemal Yelekci ^{a,*}

^a. Department of Bioinformatics and Genetics, Kadir Has University, Cibali campus, Fatih, 34083, Istanbul, Turkey

^b. Hector Institute for Translational Brain Research, Central Institute of Mental Health, Medical Faculty Mannheim, Heidelberg University, J5, 68159 Mannheim, Germany

^c. Department of Drug Science and Technology, University of Turin, via P. Giuria 9, 10125 Turin, Italy

^d. Department of Chemistry, Biology and Biotechnology, University of Perugia, via Elce di sotto 8, 06123 Perugia, Italy

^e. School of Biochemistry and Immunology, Trinity College Dublin, Dublin 2, Ireland

^f. Biochemical Laboratory, Psychiatry and Psychotherapy Department, Central Institute of Mental Health, Medical Faculty Mannheim, Heidelberg University, J5, 68159 Mannheim, Germany

*Correspondence:

Prof. Dr. Kemal Yelekçi

Department of Bioinformatics and Genetics, Faculty of Engineering and Natural Sciences,

Kadir Has University, 34083 Fatih Istanbul, TURKEY. Tel.: +90 212 533 65 32- Ext.1332; Fax:

+90 212 533 65 15; Email: yelekci@khas.edu.tr

ABSTRACT

Parkinson's disease (PD) is characterized by the loss of dopamine-generating neurons in the *substantia nigra* (SN) and *corpus striatum* (CS). Current treatments alleviate PD symptoms rather than exerting neuroprotective effect on dopaminergic neurons. New drugs targeting the dopaminergic neurons by specific uptake through the human dopamine transporter (hDAT) could represent a viable strategy for establishing selective neuroprotection. Molecules able to increase the bioactive amount of extracellular dopamine (DA), thereby enhancing and compensating a loss of dopaminergic neurotransmission, and to exert neuroprotective response because of their accumulation in the cytoplasm, are required.

By means of homology modeling, molecular docking and molecular dynamics simulations, we have generated 3D structure models of hDAT in complex with substrate and inhibitors. Our results clearly reveal differences in binding affinity of these compounds to the hDAT in the open and closed conformations, critical for future drug design. The established *in silico* approach allowed the identification of promising substrate compounds that were subsequently analyzed for their efficiency in inhibiting hDAT-dependent fluorescent substrate uptake, through *in vitro* live cell imaging experiments. Taken together, our work presents the first implementation of a combined *in silico/in vitro*-approach enabling the selection of promising dopaminergic neuron specific substrates.

Keywords: DAT, substrates, neuroprotection, virtual screening, molecular modeling,

Introduction

Parkinson's disease (PD) is the second most common neurodegenerative disorder of the central nervous system. Characteristical symptoms include tremor, rigidity and impaired movement. It is characterized by the loss of dopamine-generating neurons in the *substantia nigra* (SN) and *corpus striatum* (CS), and by the accumulation of aggregates containing α -synuclein in the brain. These protein aggregates, named Lewy Bodies, clump together at axons and dendrites in neurons in the SN. They sterically hinder the transport of neurotransmitter-filled vesicles which can no longer move along the cytoskeleton. Thus, neurotransmitter release is compromised, with a consequent gradual loss of neuronal function (Underwood and Cross, 2009). An alternative mechanism of neurodegeneration is via the chemical damage to the membrane lipids by reactive radical species, which leads to membrane leakage (Barnham et al., 2004). Both pathways contribute to the loss of cell function and neuronal death and are tightly connected (Pavlin et al., 2016).

The dopamine transporter (DAT) is an integral membrane protein and member of the neurotransmitter sodium symporters (NSS) family. It is expressed in dopaminergic neurons of the central nervous system (CNS). Its fundamental role is the rapid DA reuptake from the extracellular space and thereby termination of DA signaling. DA uptake can be maintained against very large concentration gradients, from 1 to 20 substrate molecules per second (Kristensen et al., 2011). After being taken up, enzymatic breakdown of DA to its metabolites is carried out by catechol-O-methyl transferase (COMT) and monoamine oxidase (MAO). MAO breaks down dopamine to 3, 4-dihydroxyphenylacetic acid (DOPAC) by the action of the enzyme aldehyde dehydrogenase (Juárez Olguín et al., 2016). Alternatively, cytosolic DA is taken up into vesicles by transport via the vesicular monoamine transporter 2 (VMAT2) (Wimalasena et al., 2008).

The neurotoxin MPTP (**1-methyl-4-phenyl-1,2,3,6-tetrahydropyridine**) is converted into MPP⁺ (**1-methyl-4-phenylpyridinium**) by the enzyme MAO-B. This leads to parkinsonism in primates and non-primates by selective killing of dopaminergic neurons in the SN. MPP⁺-induced neurodegeneration is specific to dopamine neurons, since after DAT-dependent uptake it accumulates in mitochondria. MPP⁺ inhibits complex I in the electron transport chain, subsequently reducing ATP production and causing oxidative stress (Wiemerslage et al., 2013). Since the death of DA neurons is the major hallmark of PD, designing new neuroprotective drugs that use this pathway to enter DA neurons may yield potential molecular targets for the treatment of PD. Using this transport pathway as a basis we may design new drugs. We can modify the structure of DAT substrates to act as antioxidants, scavenging ROS (Reactive Oxidative Spaces) (Juárez Olguín et al., 2016). Alternatively, we can add groups that are enhancing the expression of anti-apoptotic Bcl-2 (like Rasagilin) (Akao et al., 2002, p. 2). Such molecules would increase the bioactive amount of extracellular DA by competing for DAT-dependent uptake, thereby enhancing and compensating the loss of dopaminergic neurotransmission. Additionally, they may also start neuroprotective response due to their accumulation in the cytoplasm. In contrast to this, DAT inhibiting molecules may only compensate for the loss of DA signaling by reducing DA re-uptake. However, this is beyond the scope of this paper, and will be the focus of our future research. To identify promising DAT uptake-dependent candidate molecules, it is necessary to establish a reliable screening model that addresses discriminant characteristics of DAT inhibitors and

substrates. The classic alternating access model implies that the transporter protein shuttles through at least three conformational states during the transport cycle: (i) an outward-open conformation where the substrate binding pocket is accessible to the extracellular medium, (ii) an occluded conformation, where access to the pocket is blocked from either side, and (iii) an inward-facing conformation, where the pocket is open to the intracellular medium (Kristensen et al., 2011). Therefore, candidate compounds have to be screened to determine and analyze their binding characteristics to different DAT conformations. Compounds with similar structures may bind to the various conformational states of DAT during the transport cycle with different binding affinities. Such occurrences would lead to differentially effective neuroprotection based on DAT's transport capacity for a specific compound. It is thus necessary to identify the specific transporter state leading to efficient compound uptake (Kristensen et al., 2011).

In the current study we combined different *in silico* approaches i.e. homology modeling, docking, virtual screening and molecular dynamics, to identify new potential DAT substrates. We have used this approach to perform a compound screening in order to identify candidates that, based on their hDAT binding characteristics, may be substrates that are, DAT-dependently accumulated in the cytoplasm. The simulation led to the identification of 118 potential substrates. In order to verify our *in silico* results, we have monitored the effect of the six most promising candidates on hDAT-dependent fluorescent substrate (ASP+) uptake *in vitro*. *In vitro* assays with ASP+ confirmed that these compounds alter DA uptake, which means that they are competing with DA for DAT transport. One of compounds was fluorescent and was monitored inside of the DA neuron. The obtained results suggest a new way of searching DAT substrates.

Materials and Methods

Homology Modeling

The hDAT sequence was retrieved from the UniProt databank (**QO1959 SCGA3_HUMAN**) and the X-ray structure of DAT from *Drosophila melanogaster* (dDAT) from the Protein Data Bank (<http://www.rcsb.org>, PDB code: **4M48**) (Penmatsa et al., 2013). The sequences were aligned using "Align Sequences" toolkit from BIOVIA DS 4.5 (**Biovia, San Diego, USA**, <http://accelrys.com/>). The secondary structure alignment was set to TRANSMEM as for

transmembrane proteins. The model was built using “Homology Modeling” protocol in BIOVIA D.S. The first 57 and last 20 amino acids were omitted because there was no corresponding homolog to those parts, which did not affect our results since they are located far away from the binding site. These residues are mainly involved in interactions of hDAT with other proteins (Fenollar-Ferrer et al., 2014). Two sodium ions, one chlorine ion and one molecule of cholesterol were included which are important for the transport. Ten different homology models were created and verified with MODELLER plug-in included in BIOVIA DS 4.5. The model having the best DOPE and normalized DOPE score (-79899.35 and -1.3418, respectively) was selected. One loop, between Phe187 and Thr210 was refined to release the tension between amino acids using CHARMM22 force field, implemented with MODELLER plug-in in BIOVIA D.S. (MacKerell et al., 1998; Webb and Sali, 2016). The disulfide bridge between Cys180 and Cys189 was preserved. The obtained model was then minimized to avoid any steric hindrance among residue side chains. Finally, the protein was minimized and protonated at physiological pH.

Molecular docking

Three ligands, commonly used for modeling hDAT: **amphetamine** (a substrate and psychostimulant (Robertson et al., 2009)), **modafinil** (an atypical inhibitor (Madras et al., 2006)) and **cocaine** (an inhibitor) were docked into apo hDAT model with AutoDock 4.2.6 (<http://autodock.scripps.edu/>) (Morris et al., 2009). Cocaine and amphetamine were modeled with a positive charge, as they are protonated at pH=7.4. The coordinates of alpha carbon of Phe326 were used for grid-centering; grid box was set to be 50 grid points (each grid point is 0.375Å) in all directions to allow the ligand to rotate freely in binding pocket. All the compounds were situated in the central binding pocket halfway the membrane, lined by Phe155 Tyr156, Phe320, Phe326 and Ser422 residues.

To identifying the most probable open-out and closed transporter conformation, known substrates and inhibitors (**Table 1**) were docked into a set of ten conformations extracted by the MD trajectories. The number of conformations was first reduced by performing a regular sampling (one out of 100 structures) and then picking them according to the distance between Phe326 and Tyr156. In this analysis, the size of the grid box was set to be between 40 and 60 grid points depending on the size of the pocket and size of the compound.

Docking was used once more after virtual screening, to identify new possible substrates. The best candidates were docked into previously identified open-out and closed conformations.

All the compounds and proteins were prepared in BIOVIA D.S. 2016, using the “Prepare Protein” and “Prepare Ligand” protocols.

Molecular Dynamic Simulation

In order to investigate the conformational changes occurring in the transporter, hDAT, with and without substrates/inhibitors, (hDAT-amphetamine, hDAT-cocaine and hDAT-modafinil complexes and empty hDAT) were submitted to 40 ns MD simulations. The system was prepared with Visual Molecular Dynamics (VMD) (<http://www.ks.uiuc.edu/Research/vmd/>) (Humphrey et al., 1996) and all the simulations were performed with Nano Scale Molecular Dynamics (NAMD) version 2.8 (<http://www.ks.uiuc.edu/Research/namd/>) (Phillips et al., 2005). The protein was located within a **1,2-palmitoyl-oleoyl-*sn*-glycero-3-phosphocholine** (POPC) membrane (*Membrane X and Y Length* were set 100 Å for both dimensions) using the OPM web service (<http://opm.phar.umich.edu/>) (Lomize et al., 2006). The topology files for the ligands were generated using the CGENFF web service (Vanommeslaeghe et al., 2009; Yu et al., 2012). We have applied the widely used force fields: CHARMM22 for proteins and CHARMM27 for lipids in a pre-combined file to enable hybrid system. Crystallographic water molecules were preserved, and the entire system was solvated using the TIP3P water model and neutralized by addition of NaCl to an ionic concentration of 0.2 M. Cutoff local interaction distance common to both electrostatic and van der Waals calculations was set to 12 Å. A first minimization (1000 steps) was performed, keeping fixed everything (water, ions, protein, lipid head groups), except lipid tails, to induce the proper disorder of a fluid-like bilayer. After minimization velocities were reinitiated according to the desired 310 K temperature, using Langevin dynamics with damping coefficient of 5/ps. The system was then equilibrated for 0.5 ns with a 2 fs time step. A second minimization (1000 steps) was run, constraining only the protein backbone with harmonic constraints. Again, the system was equilibrated for 1ns, preventing water molecules to enter the membrane hydrophobic region. Finally, harmonic constraints were released and the entire system further equilibrated. The production run was carried out in the NPT ensemble at 310 K and 1 atm without any restraint for 40 ns. Langevin dynamics (Nose-Hoover method) was used to control fluctuations in the

barostat. (Martyna et al., 1994) From each simulation hundred frames were randomly chosen using BIOVIA DS 2016 from the last 10 ns. In order to get various results ten different frames were manually selected, based on distance between Phe320 and Tyr156, and used for the subsequent ligand docking. Known substrates and inhibitors were docked using AutoDock.

Data sets preparation

Fifty common known substrates were obtained from the literature (Cook et al., 2002; Cozzi et al., 2013; Glennon, 2014; Howell and Negus, 2014; Kohut et al., 2013; López-Arnau et al., 2012; Mavel et al., 2012; Reith et al., 2015; Rothman, 2003; Schloss et al., 2015; Seddik et al., 2013) and from the ChEMBL website (<https://www.ebi.ac.uk/chembl/>) and used to build LDA and pharmacophore-based models (Bento et al., 2014). For each substrate (classified as active molecules), the most likely tautomer and protomer at pH = 7.4 was calculated by MoKa (Milletti et al., 2010). Then, fifty decoys were generated for each substrate (active molecule) using the decoys generator tool available within the DUD-E website (<http://dude.docking.org/>) (Mysinger et al., 2012). Decoys are inactive compounds, computed based on similar physical properties but different chemical structures from substrate analogues, in order to test the validity of our model.

Twenty-five active molecules and fifty decoys were randomly selected and used to build the training set. The test set comprised all available active molecules and decoys. For the pharmacophore-based VS, alongside decoys, test set was extended with inhibitors.

The obtained models were then used to screen the Specs database, which is part of the ZINC archive (<http://zinc.docking.org/>) (Irwin et al., 2012), looking for new possible hDAT substrates. This database provides affordable molecules in terms of purity and availability (Spyrakis et al., 2013b, 2014) and contains molecules with significant chemical and geometric diversity. A set of about 300,000 compounds was downloaded and filtered based on the principles of drug-likeness using $\text{Log P} < 5$, and $150 < \text{MW} < 500$ as cut-off.

LDA-based Structure-based Virtual Screening

All VS experiments were performed with FLAP (Fingerprints for Ligands and Proteins)

developed and licensed by Molecular Discovery Ltd (<http://www.moldiscovery.com/>). Several VS campaigns were successfully performed with FLAP and are reported in the literature. (Spyrakis et al., 2013a,b, 2014) FLAP describes small molecules and protein binding sites in terms of four-point pharmacophoric fingerprints, extracted from the molecular interaction fields (MIFs) calculated by GRID (Goodford, 1985). The information contained in the MIFs is extracted and condensed in quadruplets of pharmacophoric points, used to compare, align, and superimpose different chemical entities, which can be either small molecules or macromolecules, usually described in terms of pockets.

To take into account protein flexibility in VS, the entire trajectory was clustered according to the variability of the MIFs within the pocket. The pocket was defined by FLAPsite implemented within FLAP and the MIFs calculated for all the pocket conformations generated by the dynamics. Principal Component Analysis was used to cluster the conformations and select the most representative medoids of each cluster. Ten clusters were generated and ten medoids selected to represent protein flexibility. The linear discriminant analysis approach implemented in FLAP was used to select the templates and the FLAP scores better able to discriminate between an active and decoy molecule in the training set. Different template/FLAP score combinations were used to generate LDA models then validated on the test set. Eventually, the best results in prediction were obtained with a 1 template/3 scores model, and the selected FLAP scores were H, H*DRY*N1, H*O*DRY (shape, hydrophobic interactions and hydrogen bond donor/acceptor). The same model was then used to screen the entire Specs library. When VS is carried out using an LDA model, FLAP will produce “Activity Class” predictions for each candidate, besides the usual output forms, and a corresponding LDA-R score ranking the compounds from the most active (highest score) to the most inactive (lowest score). When the inclusion of multiple structures improves VS predictions, the LDA-R score ranking gives the highest enrichment. All the operations were performed within FLAP, for a detailed description of the methodology see reference (Spyrakis et al., 2015).

The most promising 1000 compounds were selected and submitted to further pharmacophore-based virtual screening.

Pharmacophore-based VS

The pharmacophore model was built using the 50 substrates mentioned above. Pharmacophore model was created in FLAP-2.0.0 using FLAPpharm protocol (<http://www.moldiscovery.com/>). FLAPpharm generates a detailed conformational ensemble for each structure, filters these conformations to keep the ones with the most similar pharmacophore and performs a prune tree search to find common alignment models. After creating the alignment models, a pharmacophoric pseudo-molecule is generated. The model consists of the most common atomic locations as pharmacophoric points as well as MIFs and pseudo-MIFs. FLAPpharm models use a parameterized scoring function that is a weighted sum of shape, hydrophobic, hydrogen-bond donor and hydrogen-bond acceptors MIF similarities.

Molecules were aligned to each other to find the optimal MIF similarity across the set, then subsequently pharmacophore was extracted, and the least fitting molecules were excluded. By excluding these molecules, one by one, 8 pharmacophore models were created, out of which 5 had score > 1. To validate these models and to choose the best one that differentiates between active and inactive compounds, three different datasets were created. One dataset contained 50 substrates and 77 inhibitors (Cook et al., 2002; Cozzi et al., 2013; Glennon, 2014; Howell and Negus, 2014; Kohut et al., 2013; López-Arnau et al., 2012; Mavel et al., 2012; Reith et al., 2015; Rothman, 2003; Schloss et al., 2015; Seddik et al., 2013), second dataset contained 50 substrates and 2500 decoys and the third dataset contained all three. Since we are interested in finding substrates only, we marked substrates as active while both inhibitors and decoys were marked as inactive compounds. Model was chosen according to the LBVS enrichment.

The best performing model was used to further screen the 1000 compounds coming from the SBVS. Accuracy was set to the second highest. The first 150 candidates (according to GlobSum) were docked into the open and closed hDAT conformation. The six commercially available compounds (Spects) having better ΔG values for closed hDAT conformation were sourced for our *in vitro* analysis.

To identify new possible substrates, top 150 compounds obtained after virtual screening were docked into previously identified open-out and closed conformations. In this analysis, the grid box was centered to CA atom of Phe320 and the size of the grid box was set to be 50 grid points for all the candidates.

Chemicals

Compounds **1**, **2**, **3**, **4**, **5** and **6** were purchased from Specs (Zoetermeer, The Netherlands). **4-(4-(dimethylamino) styryl)-N-methylpyridinium iodide (ASP+)** was purchased from Life Technologies. All other chemicals were from Sigma-Aldrich.

HEK-hDAT cell culture and ASP+ uptake

The HEK293 cells stably expressing the recombinant human DAT (HEK-hDAT) (Hummerich et al., 2004) were maintained in Dulbecco's modified Eagle's medium supplemented with 10% fetal bovine serum, penicillin (100U/mL), streptomycin (100µg/mL), and geneticin (G418, 200µg/mL) at 37°C in 95% humidified air with 5% CO₂. The HEK-hDAT cells were incubated for 10 min with compounds 1, 2 or 3 (0µM-30µM) at 37 °C. Subsequently, the cells were loaded with ASP+ for 30 s. The cells were washed with medium before imaging. The ASP+ was added at the concentration of 10 µM, as previously reported (Lau et al., 2015). Mouse ES cell-derived dopaminergic neurons were generated as described by Martí and colleagues (Martí et al., 2017). Briefly, the growth-factor-based differentiation protocol comprised three stages: (1) generation of neuronal stem spheres, (2) selection of dopaminergic progenitors, and (3) terminal differentiation of dopaminergic neurons. During stage 1 and 2, culture medium was supplemented with growth factors that drive neuronal differentiation along the dopaminergic pathway. Terminal differentiation was induced by withdrawal of growth factors and yielded mature neurons after 14 days. Overall, differentiation from stem cell to mature neurons took 28 days. ES cell-derived dopaminergic neurons were incubated with compound 6 for 10 min at 37°C before image acquisition.

Image Acquisition and Data Analysis

Images and data analyses for experiments with ASP+ were performed as described previously (Lau et al., 2015). Live-cell imaging of HEK-hDAT cells was performed using a Leica TCS SP5 imaging system attached to a DM IRE2 microscope equipped with an incubation chamber (Ibidi, Planegg, Germany). Excitation laser was a DPSS laser (561nm). Confocal z-stacks were acquired with sections taken every 0.5 µm with a 63× magnification. During image acquisition of control ASP+ fluorescence intensities, the photomultiplier sensitivity was set to acquire non-saturated pixel value to allow quantitative image acquisition. To ensure

quantitative ASP+ imaging for dose response tracing, images of each respective compound were acquired with their own internal controls. Images were exported as tiff-files and imported to NIH ImageJ (NIH, Bethesda, USA) for quantification of ASP+ fluorescence intensities. Regions of interest (ROI) were selected with the freehand selection tool. For all ROIs, the integrated fluorescence densities were determined after cutting off background fluorescence. Data from at least 10 regions of interest (ROI) were averaged for each 35mm μ -dish imaged (Ibidi, Planegg, Germany) (Martí et al., 2017). ASP+ fluorescence intensities provided in results and shown in **Figure 5** are given as the mean \pm SEM. Statistical analysis was performed by one-way ANOVA followed by post hoc Tukey tests using GraphPad Prism software (GraphPad Software, Inc., La Jolla, USA). $P < 0.05$ was considered significant. Each set of experiments was performed three times.

RESULTS

Establishing a new homology model for hDAT

First, we established a new homology model for hDAT based on its known amino acid sequence and the homology of hDAT and dDAT. The sequence identity and similarity between dDAT and hDAT was estimated to be 49.6% and 69.2%, respectively (**Figure 1**). Our model represented hDAT in outward open conformation. Outer (between Asp476 and Arg85) and inner (between Phe320 and Tyr156) extracellular gates were opened, while intracellular gate (between Asp436 and Arg60) was closed agreeing with the published results (Cheng et al., 2015; Cheng and Bahar, 2015). The disulfide bridge between Cys180 and Cys189 was maintained. In order to get a more precise model for structure-based drug design we have extended the homology model of hDAT using molecular dynamics simulation, to find 2 conformational structures open-out, inhibitor-bound and closed, substrate bound.

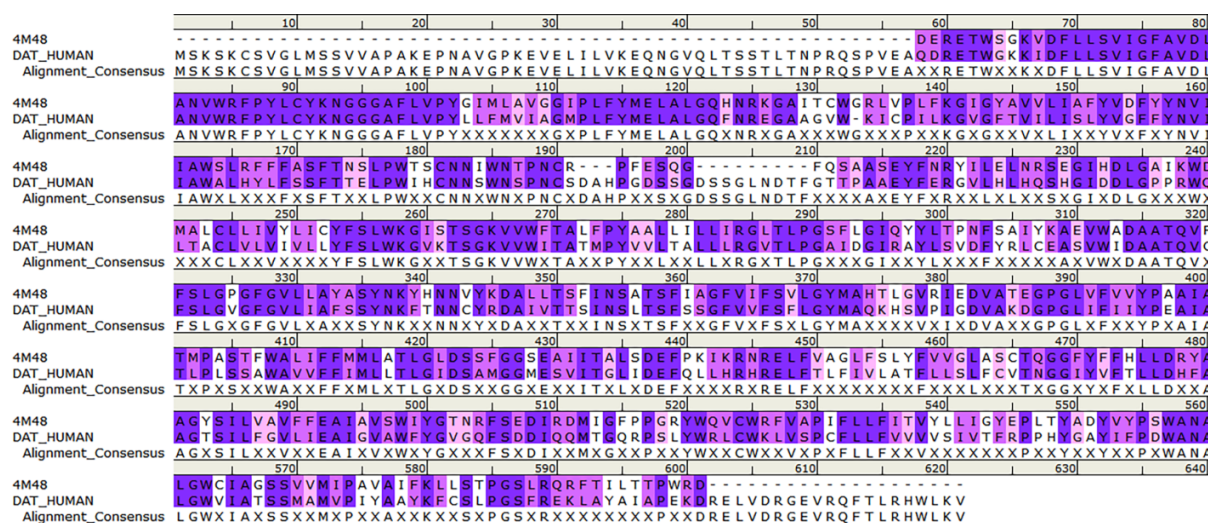


Figure 1. Sequence alignment: Sequence alignment of the dDAT (4M48) and hDAT (purple = identical amino acids, magenta = similar amino acids, pink = less similar amino acids, white = no match of amino acids).

The stability of hDAT was evaluated by root-mean-square-deviation (RMSD) from the initial structure and by residue root-mean-square-fluctuation (RMSF) values (**Supporting Info. S1**). The RMSD stabilized around 4 Å (for all the simulations) from the reference conformation after approximately 5000 time steps (10 ns). From the RMSF measurement we reasonably observed that the most flexible residues were located in the extracellular loops. The conformations later used for docking simulations were taken after RMSD stabilization. The first differences between inhibitors and substrates binding kinetics was noticed after 20 ns (10,000 steps).

After stabilization of RMSD in the hDAT-substrate complex, we noticed closing of the residues of the binding pocket only in presence of amphetamine (**Figure 2a**). Specifically, residue Phe320 closes the gate above the substrate and induces the tilting of the TM6 region (**Figure 3a and 3b**). We also observed dehydration of the binding pocket due to hydrophobic interactions of Phe155, Tyr156, Phe320 and Phe326. For visualization of the interactions we used pictures generated in BIOVIA Discovery Studio 2016 (**Figure 2**).

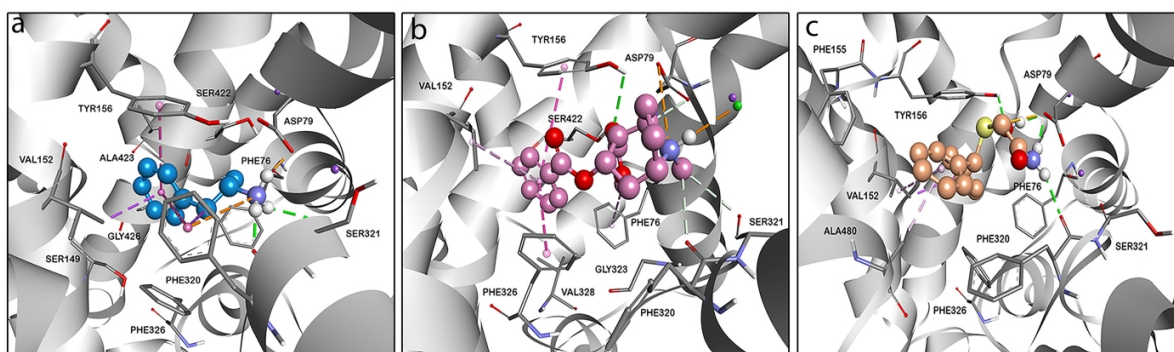


Figure 2. Ligand interactions with hDAT Snapshot of key molecular interactions (green – Hydrogen bond, pink – Van der Waals, orange - electrostatic) of amphetamine (a), cocaine (b) and modafinil (c) with hDAT in a close conformation. While binding of amphetamine (a) causes flipping of Phe320 in the hDAT, cocaine (b) and modafinil (c) binding maintain an outward-open conformation in the hDAT.

Comparison of hDAT-ligand conformations using visual molecular dynamics

A comparison of the substrate bound structure with the inhibitor bound structure and empty DAT structure showed that the distance between Phe320 and Tyr156 decreases. These two aminoacids are located above the binding site, and are closing the gate after the substrate binding (**Figure 3**). In particular, for amphetamine-hDAT complex the distance, upon structure stabilization, is maintained around 5 Å, while in all other cases it is around 13 Å (**Figure 4a**). The fact that amphetamine (substrate) binding causes the decrease in size of the pocket may suggest that the substrate binding is necessary to cause a conformational change. The lower Solvent Accessible Surface Area (SASA) of amino acids lining the binding pocket (Phe76, Val78, Asp79, Ser142, Val152, Gly153, Tyr156, Phe320, Ser321, Phe326, Val328 and Ser422) was also measured in VMD with a probe radius of 1.4 Å (**Figure 4b**). The results show lower SASA of residues in the binding pocket when a substrate, rather than when an inhibitor, is bound.

Overall, the main differences between amphetamine-hDAT complex and others (empty hDAT and cocaine-hDAT and modafinil-hDAT complexes) were a flipping of the Phe320 side chain, a decreased distance between Phe320 and Tyr156 and a decreasing of solvent accessible surface area.

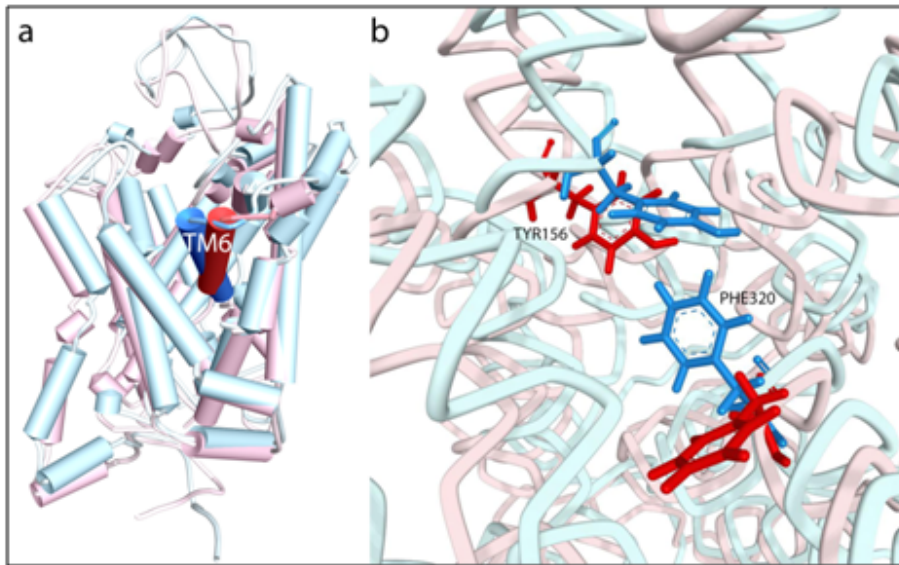


Figure 3. Superimposition of hDAT open and hDAT closed (a) superimposed hDAT open (red) and hDAT closed (blue) showing tilting of TM6 domain; (b) Phe320 and Tyr156 are closing the gate of the binding pocket in the hDAT closed conformation (blue), while the gate remains open in the hDAT open conformation (red).

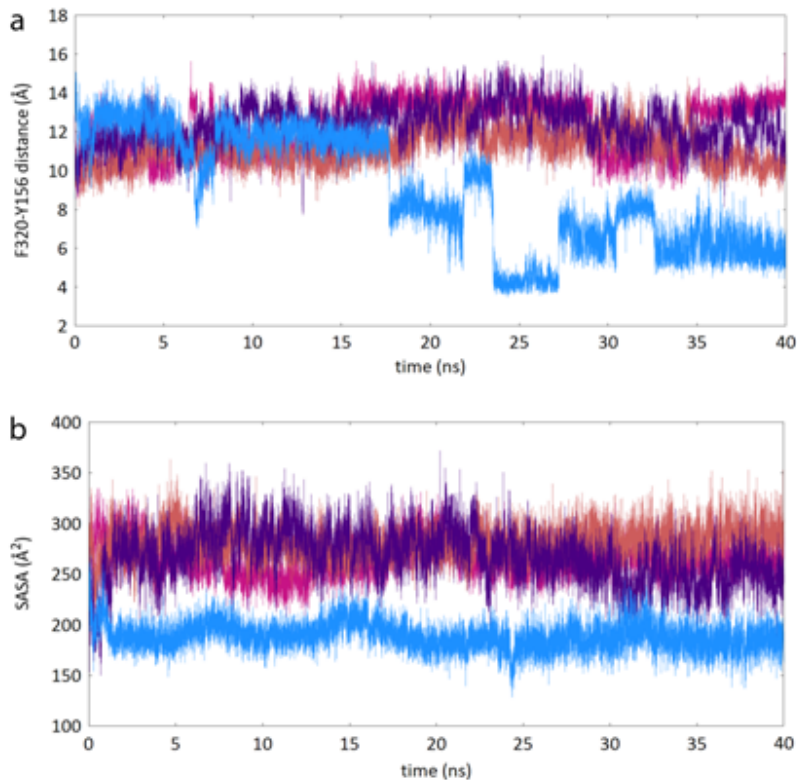


Figure 4. Comparison of distance between two main amino acid residues and SASA

(a) Comparison of F320 and Y156 distance in hDAT-amphetamine (blue), hDAT-cocaine (pink), hDAT-modafinil (orange) complexes and empty hDAT (purple) transporter. Amphetamine decreases the F320 to Y156 distance when bound to hDAT. (b) Comparison of SASA values shows that the hDAT- amphetamine complex (blue) displaces H₂O from the binding pocket whereas the hDAT-cocaine (pink), hDAT-modafinil (orange) complexes and empty hDAT (purple) maintain H₂O in the binding pocket.

Search for the best open and closed conformation of hDAT-interacting compounds by molecular docking

From previous findings (Celik et al., 2008; Wang et al., 2015) we can speculate that if a compound is a substrate, it has a higher affinity for the closed conformation. On the other hand if this compound is an inhibitor (preventing the transporter from moving into the closed conformation) it should have a high affinity for open conformation and low or no affinity for the closed conformation. To identify the most suitable hDAT open-out and closed conformations to perform docking experiments with inhibitors and substrates, we collected 10,000 frames from the last 10 ns of simulation. One hundred frames were randomly chosen by BIOVIA D.S. 2016. Based on the distance between Phe320 and Tyr156, 10 frames were manually picked for evaluation. Known substrates and inhibitors were docked in the 10 possible conformations extracted from each trajectory, to determine those better able to discriminate among the two classes of compounds (See Materials and Methods for further details). The free energy values, calculated by Autodock, are reported in **Table 1**. In accordance with the known literature, inhibitors generated more stable complexes within the open conformation, while there was very low or no affinity at all (positive ΔG values) for the closed conformation. Contrary to this, substrates showed good affinity for both conformations but were shown to be better stabilizing the closed form of the transporter.

Compounds	hDATopen	hDAT closed
	ΔG (kcal/mol)	ΔG (kcal/mol)
SUBSTRATES		
Neurotransmitters		
dopamine	-4.61	-6.22
noradrenalin	-4.71	-5.47
serotonin	-5.7	-6.66
Amphetamines and its derivatives		

amphetamine	-5.22	-6.11
cathinon	-5.12	-6.3
metcathinone	-5.19	-6.41
MDA	-5.9	-6.76
metamphetamine	-5.72	-5.58
Neurotoxins and related compounds		
MPP+	-5.72	-6.28
ASP+	-6.43	-4.57
6-OH-dopamine	-5.72	-5.58
INHIBITORS		
Nonselective transporter inhibitors		
cocaine	-8.31	-2.39
duloxetine	-8.69	-3.41
modafinil	-7.87	-5.15
nefazodine	-9.46	98.96
trimipramine	-8.2	3.3
Selective Dopamine transporter inhibitors		
altropan	-8.33	10.27
DBL-583	-8.19	448
GBR-12783	-10.53	69.3
RTI-229	-9.52	5
vanorexine	-9.77	89
GYKI-52895	-8.27	42.02
Selective Serotonin reuptake inhibitors		
escitalopram	-7.42	5.74
sertalin	-9.19	7.99
sibutramin	-7.61	-0.87

Table 1. Known substrates and inhibitors docked in open and closed conformation; ΔG – free energy of binding.

Identification of promising hDAT substrate candidates

To identify new compounds possibly recognized and transported by hDAT as substrates we combined three different approaches in a pipeline, consisting of flexible Linear Discriminant Analysis (LDA)-based VS, pharmacophore-based VS and docking simulations.

Based on the belief that the inclusion of flexibility in VS generally provides more reliable results (Hou et al., 2015; Moroy et al., 2015; Sinko et al., 2011; Spyraakis and Cavasotto, 2015; Totrov and Abagyan, 2008), we performed a first flexible VS campaign using a recently

published methodology, based on the integrated molecular dynamics (MD) and the FLAP algorithm (Spyrakis et al., 2015). The transporter flexibility was investigated by means of MD simulation performed on the amphetamine-hDAT complex (closed conformation). Then, for all the possible binding site conformations, the Molecular Interaction Fields (Kador et al., 1985) were calculated with FLAP (Baroni et al., 2007) and clustered through principal component analysis. The Linear Discriminant Analysis-based protocol implemented in FLAP was applied to automatically choose the combination of conformational templates and FLAP scores better able to discriminate between active compounds and decoys in a training set (see Methods for further details). Previous analyses reported a 3 template over 3 FLAP-score combination as the one able to provide the best overall and early enrichment (Spyrakis et al., 2015). Clearly, the number of templates and FLAP-scores strictly depend on the nature of the target and its intrinsic flexibility. In this specific case a model combining one MD-generated template and three different FLAP-scores provided the best enrichment when used to screen the test set. The enrichment increase obtained with respect to a single receptor conformation VS performed with the starting model was particularly relevant. The overall AUC (Area Under the Curve) moved from 0.57 to 0.91 and the partial ROC (Receiver Operating Characteristic) enrichment at 1% and 5% moved from 0.04 and 0.10 to 0.14 and 0.71, respectively. The model was thus used to screen the Specs database (part of the ZINC database) looking for new potential hDAT substrates. The best scored thousand compounds, according to the LDA-R score, were selected and submitted to the following pharmacophore-based VS. (see Materials and Methods for further details)

Our pharmacophore model, based on chemical characteristics of substrates (see Materials and Methods for further details), was able to distinguish between substrates and inhibitors, as well as decoys. GlobSum probe was showing good enrichment, both in differentiating between substrates and decoys ($AUC_{(100\%)} = 0.92$; $AUC_{5\%} = 0.66$); substrates and inhibitors ($AUC_{(100\%)} = 0.96$; $AUC_{5\%} = 0.95$); and between both substrates against decoys and inhibitors ($AUC_{(100\%)} = 0.92$; $AUC_{5\%} = 0.64$) which is why GlobSum was chosen to rank the compounds. The most promising 150 molecules coming from the pharmacophore-VS were docked in the open-out and closed form of the transporter previously selected. 118 out of 150 molecules confirmed the supposed substrate nature, according to the docking results. The six compounds showing favorable free energy values when docked in closed hDAT are reported in **Table 2**.

To confirm the *in silico* predictions the six compounds were analyzed *in vitro* to verify their capability of alter the hDAT-dependent uptake of **4-(4-diethylaminostryryl)-N-methylpyridinium iodide (ASP+)**, and thus proving their interaction with the hDAT transporter. The four most promising candidates that have also shown activity *in vitro* are shown in **Figure 5**.

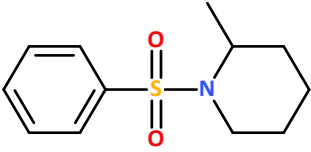
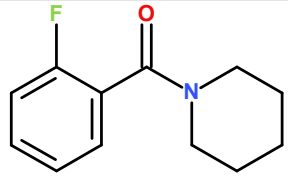
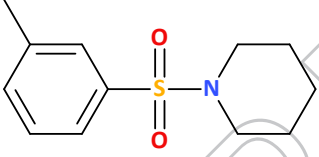
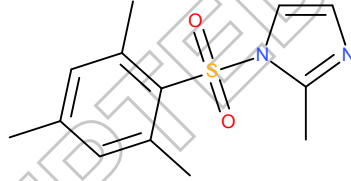
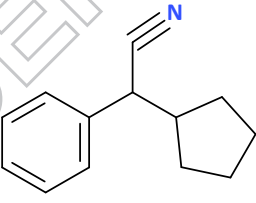
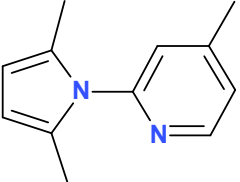
Compounds		hDAT open	hDAT closed
		ΔG (kcal/mol)	ΔG (kcal/mol)
Compound 1		-6.08	-7.59
Compound 2		-5.5	-6.9
Compound 3		-6.22	-7.15
Compound 4		-6.26	-6.97
Compound 5		-5.76	-7.08
Compound 6		-5.38	-6.58

Table 2: Best hDAT potential substrates obtained from VS docked in closed and open conformations.

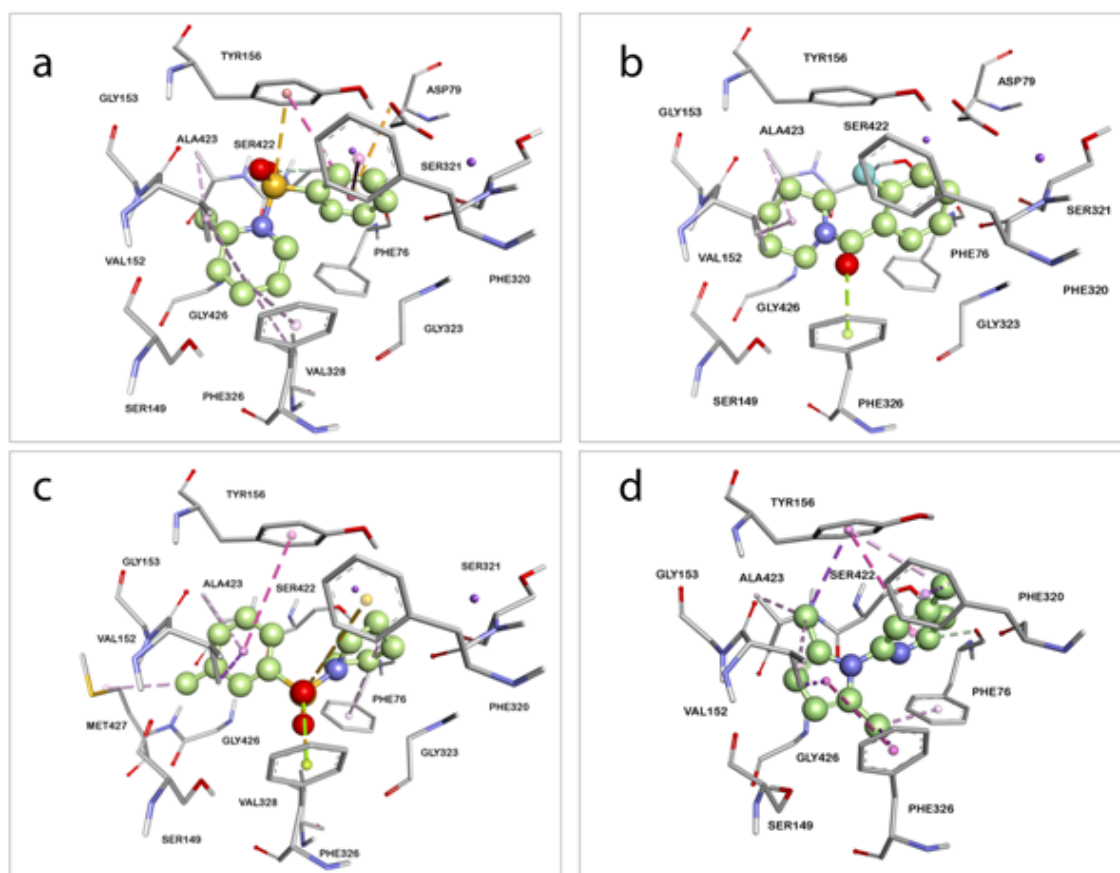


Figure 5. Interactions of ligands with hDAT Predicted interactions of compounds **1** (a), **2** (b), **3** (c) and **6** (d) in binding pocket of hDAT in closed conformation.

Compounds compete with DAT-dependent ASP⁺ uptake in vitro

The fluorescent organic compound ASP⁺ is a substrate for the monoamine transporters that has been applied in various studies to visualize neurotransmitter uptake in monoaminergic neurons in real-time live cell imaging, including DAT-dependent uptake of dopamine (Inyushin et al., 2013; Lau et al., 2015; Matthaeus et al., 2015; Oz et al., 2010; Schwartz et al., 2003). Here we applied ASP⁺ live cell imaging to determine whether our compounds compete with ASP⁺ as substrates for DAT *in vitro* and thereby decrease the amount of detectable ASP⁺ fluorescence.

Initially we have tested six compounds in ASP+ live cell imaging experiments to quantify to which extent they influence ASP+ uptake in human embryonic kidney cells expressing the hDAT (HEK-hDAT; **Figure 6a**). For this experiment we have chosen to apply 30 μM of each compound, which is 3 times the concentration required to inhibit ASP+ uptake by the DAT substrates d-amphetamine and dopamine (Zapata et al., 2007). This experiment showed that compounds **1 - 3** had the strongest effect on ASP+ uptake by HEK-hDAT, which was significantly diminished to approximately 40% for compound **1**, 60% for compound **2** and compound **3** (all compounds $p < 0.001$ vs control intensity). Compound **4** and **5** showed a less significant reduction compared to controls ($p = 0.0037$ for compound **4**, and $p = 0.0024$ for compound **5**). With regard to compound **6** we were not able to determine an alteration of ASP+ uptake in HEK-hDAT. Since we have detected weak fluorescence intensities in the absence of ASP+ (data not shown), we have incubated compound **6** in dopaminergic neurons derived from mouse embryonic stem cells (Martí et al., 2017). **Figure 6b** shows exemplary live cell images of compound **6**-labelled dopaminergic neurons, in which the compound predominantly stained globular structures on the soma and along neurites.

To further characterize compound **1 - 3**, HEK-hDAT cells were incubated with each compound (0 μM-30 μM) for 10 min prior addition of 10 μM ASP+ to the imaging chamber. As shown in **Figure 6c**, the presence of compound **1** significantly dose-dependently diminished ASP+ uptake. A decreased ASP+ fluorescence to $50\% \pm 2.67$ of control values (SEM given) was measured at for 3 μM compound **1**, and was maintained for higher concentrations (10 μM: $41\% \pm 2.42$; 30 μM: $38\% \pm 2.25$). In presence of compound **2**, already 1 μM was enough to significantly diminish ASP+ fluorescence substrate (**Figure 6d and Supporting Info. S2**). At 1 μM, ASP+ fluorescence decreased to $60\% \pm 2.44$ (SEM given) compared to control intensities. This fluorescence intensity remained alike when using higher concentrations of compound **2** (3 μM: $56\% \pm 2.48$; 10 μM: $55\% \pm 2.09$; 30 μM: $64\% \pm 2.39$). Finally, incubation of HEK-hDAT with compound **3** also revealed a significant decrease of ASP+ uptake with increasing concentrations of the compound (**Figure 6e**). A significant reduction of ASP+ fluorescence started at 3 μM (76 ± 3.34 ; SEM given) and slightly increased at higher concentration with 30 μM showing the strongest ASP+ uptake alteration compared to control conditions (10 μM: 77 ± 4.09 ; 30 μM $57\% \pm 4.35$).

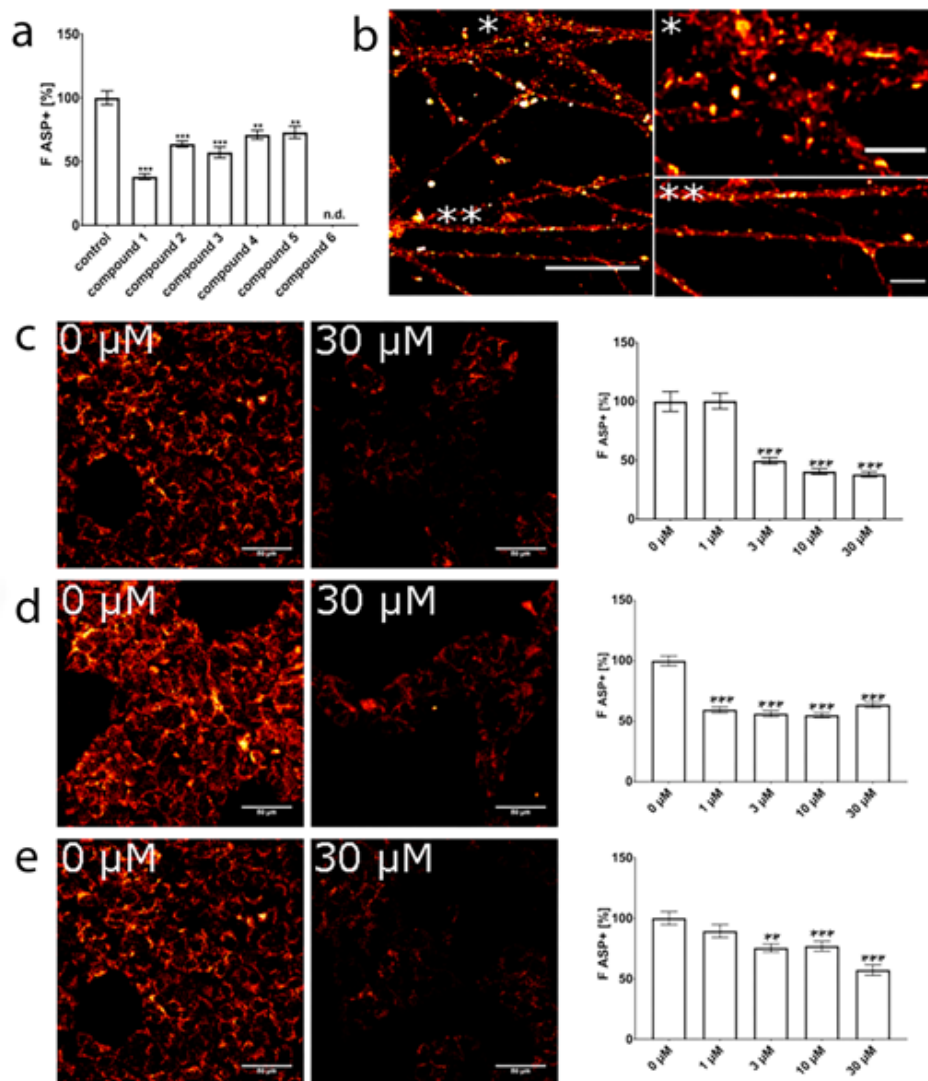


Figure 6. Live cell imaging of hDAT-dependent ASP+ uptake into HEK-hDAT cells.

(a) HEK-hDAT were incubated for 10 min with 30 μM of each compound prior addition of ASP+. Compounds 1 – 3 showed a significantly stronger effect on ASP+ uptake (***, $p < 0.001$) compared to compound 4 and 5. An effect of compound 6 could not be determined (n.d.) since the compound proved to be fluorescent when microscope settings for acquiring ASP+ images were applied. (b) Exemplary images of compound 6 fluorescence in ES cell-derived dopaminergic neurons. Compound 6 fluorescence was found in globular, roundish as well as elongated structures in the soma and neurites. Scale bar: 50 μM. * shows the enlarged soma of a neuron, scale bar: 15 μm. ** shows enlarged neurites, scale bar: 15 μm. (C-E) HEK-hDAT were incubated for 10 min with different

concentrations of the respective compound (0 – 30 μ M) prior addition of ASP+. Compounds **1** (c), **2** (d), and **3** (e) competed with hDAT-dependent ASP+ uptake and significantly reduced ASP+ fluorescence intensities. Representative confocal ASP+ fluorescence images of HEK-hDAT are shown in absence (0 μ M; control fluorescence intensity) and in presence of the respective compound (30 μ M; highest concentration applied). Bars represent means \pm SEMs of $N \geq 50$ ROIs taken from $N=3$ independent experiments. ** $p \leq 0.01$, *** $p \leq 0.001$.

Discussion

Before the release of the X-ray structure of drosophila's DAT (dDAT) (Penmatsa et al., 2013), NSS transporters have been modeled on the structure of bacterial leucine transporter (LeuT) (Yamashita et al., 2005), having with it an overall sequence similarity of about 20-25% (Beuming et al., 2006; Forrest et al., 2006; Indarte et al., 2008; Rayna et al., 2006). LeuT and dDAT have several major differences, such as a kink in TM12 halfway across the membrane bilayer, a latch-like C-terminal domain that caps the cytoplasmic gate and a cholesterol molecule in the groove formed by TMs 1a, 5 and 7. The dDAT also co-transport a chloride anion with substrate, a peculiarity not shared by LeuT (Kantcheva et al., 2013). After the dDAT structure release, a new homology model of hDAT has been recently published (Cheng et al., 2015; Cheng and Bahar, 2015) proving higher reliability with respect to the previous ones. Following this strategy, we have created a new homology model of the human dopamine transporter, to have a more precise model for structure based drug design purposes.

We speculated that since the inhibitors block the transporter in an outward open conformation (Schmitt et al., 2013), they could be docked more favorably in it, rather than in the closed conformation. On the other hand, the substrate should be able to bind the outward-open, the closed and the inward-open conformation. Accordingly, finding open and closed conformations of hDAT is helpful in the design of next generation anti-parkinsonian drugs. We have investigated the conformational changes occurring in hDAT upon the binding of a substrate or inhibitors, mainly related to the closing of the pocket mediated by Phe320. These findings agree with X-ray structures published recently (Wang et al., 2015). A previous study suggested that modafinil, which acts as an atypical inhibitor, keeps the hDAT in a closed conformation (Schmitt et al., 2013). However, our results suggest that both cocaine and modafinil keep the transporter in an outward-open conformation, whereas amphetamine causes closing of transporter. Furthermore, we suggest that cocaine and modafinil form more non-bonded interactions with hDAT which results in stronger binding affinity. The inhibitor

keeps the transporter in the same conformation as the empty transporter. In hDAT-amphetamine complex we have observed the closure of the outer extracellular gate between Asp476 and Arg85 amino acids, and inner extracellular gate (Phe320 and Tyr156). After 40 ns simulation, we did not observe any major changes in the system that led to conformational change from occluded to inward-open conformation. The increase in distance between amino acids of the intracellular gate (Asp436 and Arg60) was not significant, so we speculated that there must be something else causing it, like binding of another substrate (Koldso et al., 2013) or sodium being dragged by electrochemical gradient (Cheng and Bahar, 2015; Tavoulari et al., 2016), but this is beyond of the scope of these research. **(Supporting Info. S3)** Furthermore, conformations that we have identified could be used for computational modeling. Using docking into these two conformations can indicate whether the compound is an inhibitor or a substrate. Based on docking of the known compounds into these two conformations we have determined differences between them. Namely, substrates show binding energies at around -7 kcal/mol (or more positive) for both hDAT conformations. The inhibitors show around -8 kcal/mol (or more negative) for open conformation and much less, or no binding for closed conformation (**Table 1**). Lastly, we found a method to screen specifically for substrates, and we conclude that the best way is to take both protein conformations and ligands chemical properties into account.

In silico screening led us to choose six promising molecules out of 300,000 compounds, which indeed showed an effect on hDAT ASP⁺ transport *in vitro*. ASP⁺ has been shown to be translocated through plasma membrane not only by selective high-affinity transporters like DAT or SERT but also by low-affinity, high capacity monoamine transporters like OCT (organic cation transporter) and PMAT (plasma membrane monoamine transporter) and in addition by yet unknown uptake mechanisms.²³ Hence, the ASP⁺ transport rate mediated by high affinity transporters observed in different cellular systems accounts up to maximally 50 – 60 % of total accumulation into the cells. Therefore, it is not possible to calculate accurate IC₅₀ values for the three most competing compounds. Rather we show that these compounds tested in our *in vitro* section inhibit ASP⁺ uptake to about 50% at concentrations within the same order of magnitude as do the compounds in the computational calculations, i.e. the low micro-molar range. Our *in vitro*-experiments also identified one compound as a fluorescent DAT substrate, which is taken up into mouse ES cell-derived neurons and localizes to

globular and slightly elongated structures, yet to be identified. In summary, this proves that the combination of *in silico* and *in vitro* studies is very effective and less time consuming and this approach can be used in the future to search for novel potent neuroprotective drugs that target dopaminergic neurons. In our future research, we will repeat the same procedure on recently published X-ray structure of hSERT (Coleman et al., 2016), in order to check the selectivity of our compounds. After entering and accumulating in dopaminergic neurons, these compounds could target various proteins involved in neuroprotective or immunological mechanisms. They could target Monoamine Oxidase (MAO-B inhibitors), Glyceraldehyde-3-phosphate dehydrogenase (GADPH) or cytochrome c, among others. Alternatively, these compounds could bind heavy metal ions, calcium ions or ROS (Akao et al., 2002; Juárez Olguín et al., 2016; Pavlin et al., 2016). Some authors have also suggested that the usage of DAT substrates could also be helpful for the treatment of cocaine addiction and might ameliorate the symptoms of stimulant withdrawal, thereby, facilitating abstinence (Blough et al., 2014; Rothman, 2003). Continuing our work, we will screen these compounds for possible activities on enzymes in the cell (such as MAO, GADPH, caspases, cytochrome c, etc.) responsible for neurodegeneration/protection and look for other compounds able to target at the same time the hDAT transporter and other relevant proteins.

Conclusion

In conclusion, we have shown that *in silico* screening with our hDAT homology model results in identification of hDAT-binding compounds that can be classified either as substrates or inhibitors based on their binding characteristics to the open-out or closed hDAT conformation. The interaction of hDAT and specific compounds, identified as hDAT substrates *in silico*, can be verified *in vitro* by analyzing their effect on hDAT-dependent ASP⁺ uptake in presence of the respective compound. Furthermore, our *in silico* model provides the potential to screen for compounds targeting other important mechanisms in dopaminergic neurodegeneration. Compounds being identified with our model may be applied as templates to design new neuroprotective substrates that are specifically targeting dopaminergic neurons.

ASSOCIATED CONTENT

Supporting Information S1: RMSD and residue RMSF values after 40 ns MD simulation.

Supporting Information S2: Alteration/inhibition of ASP+ uptake into HEK-hDAT cells.

Supporting Information S3: Behaviour of amino acids of DATs gates over time in apo hDAT and hDAT-amphetamine complex

Acknowledgement

This work was sponsored by Marie Curie Fellowship, Training in Neurodegeneration, Therapeutics, Intervention and Neurorepair (TINTIN); Funding Scheme: FP7-MC-ITN with grant number: 608381. The work of TL is funded by the H.W. & J. Hector Stiftung.

TD, KY, YM and PS were funded by Marie-Sklodowska-Curie action project No. 608381, funding scheme FP7-MC-ITN. TL is funded by the H.W. & J. Hector Stiftung. The funders were not involved in design of the study or writing of the manuscript.

Author Contributions

The manuscript was written through contributions of all authors. All authors have given approval to the final version of the manuscript. T.D and K. Y. conceptualized the research; F.S. and P.B. contributed to in silico screening; Y.M., T.L. and P. S. contributed to in vitro studies. G.D. improved the manuscript text and contributed with his invaluable comments.

Conflict of Interest

The authors declare no conflict of interest.

References

- Akao, Y., Maruyama, W., Yi, H., Shamoto-Nagai, M., Youdim, M.B., Naoi, M., 2002. An anti-Parkinson's disease drug, N-propargyl-1 (R)-aminoindan (rasagiline), enhances expression of anti-apoptotic bcl-2 in human dopaminergic SH-SY5Y cells. *Neurosci. Lett.* 326, 105–108.
- Barnham, K.J., Masters, C.L., Bush, A.I., 2004. Neurodegenerative diseases and oxidative stress. *Nat. Rev. Drug Discov.* 3, 205–214. <https://doi.org/10.1038/nrd1330>
- Baroni, M., Cruciani, G., Sciabola, S., Perruccio, F., Mason, J.S., 2007. A Common Reference Framework for Analyzing/Comparing Proteins and Ligands. Fingerprints for Ligands And Proteins (FLAP): Theory and Application. *J. Chem. Inf. Model.* 47, 279–294. <https://doi.org/10.1021/ci600253e>
- Bento, A.P., Gaulton, A., Hersey, A., Bellis, L.J., Chambers, J., Davies, M., Krüger, F.A., Light, Y., Mak, L., McGlinchey, S., Nowotka, M., Papadatos, G., Santos, R., Overington, J.P., 2014. The ChEMBL

- bioactivity database: an update. *Nucleic Acids Res.* 42, D1083–D1090.
<https://doi.org/10.1093/nar/gkt1031>
- Beuming, T., Shi, L., Javitch, J.A., Weinstein, H., 2006. A Comprehensive Structure-Based Alignment of Prokaryotic and Eukaryotic Neurotransmitter/Na⁺ Symporters (NSS) Aids in the Use of the LeuT Structure to Probe NSS Structure and Function. *Mol. Pharmacol.* 70, 1630–1642.
<https://doi.org/10.1124/mol.106.026120>
- Blough, B.E., Landavazo, A., Partilla, J.S., Decker, A.M., Page, K.M., Baumann, M.H., Rothman, R.B., 2014. Alpha-ethyltryptamines as dual dopamine–serotonin releasers. *Bioorg. Med. Chem. Lett.* 24, 4754–4758. <https://doi.org/10.1016/j.bmcl.2014.07.062>
- Celik, L., Schiøtt, B., Tajkhorshid, E., 2008. Substrate Binding and Formation of an Occluded State in the Leucine Transporter. *Biophys. J.* 94, 1600–1612. <https://doi.org/10.1529/biophysj.107.117580>
- Cheng, M.H., Bahar, I., 2015. Molecular Mechanism of Dopamine Transport by Human Dopamine Transporter. *Structure* 23, 2171–2181. <https://doi.org/10.1016/j.str.2015.09.001>
- Cheng, M.H., Block, E., Hu, F., Cobanoglu, M.C., Sorkin, A., Bahar, I., 2015. Insights into the Modulation of Dopamine Transporter Function by Amphetamine, Orphenadrine, and Cocaine Binding. *Front. Neurol.* 6. <https://doi.org/10.3389/fneur.2015.00134>
- Coleman, J.A., Green, E.M., Gouaux, E., 2016. X-ray structures and mechanism of the human serotonin transporter. *Nature* 532, 334–339. <https://doi.org/10.1038/nature17629>
- Cook, C.D., Carroll, F.I., Beardsley, P.M., 2002. RTI 113, a 3-phenyltropane analog, produces long-lasting cocaine-like discriminative stimulus effects in rats and squirrel monkeys. *Eur. J. Pharmacol.* 442, 93–98.
- Cozzi, N.V., Brandt, S.D., Daley, P.F., Partilla, J.S., Rothman, R.B., Tulzer, A., Sitte, H.H., Baumann, M.H., 2013. Pharmacological examination of trifluoromethyl ring-substituted methcathinone analogs. *Eur. J. Pharmacol.* 699, 180–187. <https://doi.org/10.1016/j.ejphar.2012.11.008>
- Fenollar-Ferrer, C., Stockner, T., Schwarz, T.C., Pal, A., Gotovina, J., Hofmaier, T., Jayaraman, K., Adhikary, S., Kudlacek, O., Mehdipour, A.R., Tavoulari, S., Rudnick, G., Singh, S.K., Konrat, R., Sitte, H.H., Forrest, L.R., 2014. Structure and Regulatory Interactions of the Cytoplasmic Terminal Domains of Serotonin Transporter. *Biochemistry (Mosc.)* 53, 5444–5460. <https://doi.org/10.1021/bi500637f>
- Forrest, L.R., Tang, C.L., Honig, B., 2006. On the Accuracy of Homology Modeling and Sequence Alignment Methods Applied to Membrane Proteins. *Biophys. J.* 91, 508–517.
<https://doi.org/10.1529/biophysj.106.082313>
- Glennon, R.A., 2014. Bath Salts, Mephedrone, and Methylenedioxypyrovalerone as Emerging Illicit Drugs That Will Need Targeted Therapeutic Intervention, in: *Advances in Pharmacology*. Elsevier, pp. 581–620.
<https://doi.org/10.1016/B978-0-12-420118-7.00015-9>
- Goodford, P.J., 1985. A computational procedure for determining energetically favorable binding sites on biologically important macromolecules. *J. Med. Chem.* 28, 849–857.
<https://doi.org/10.1021/jm00145a002>
- Hou, X., Li, K., Yu, X., Sun, J., Fang, H., 2015. Protein Flexibility in Docking-Based Virtual Screening: Discovery of Novel Lymphoid-Specific Tyrosine Phosphatase Inhibitors Using Multiple Crystal Structures. *J. Chem. Inf. Model.* 55, 1973–1983. <https://doi.org/10.1021/acs.jcim.5b00344>
- Howell, L.L., Negus, S.S., 2014. Monoamine Transporter Inhibitors and Substrates as Treatments for Stimulant Abuse, in: *Advances in Pharmacology*. Elsevier, pp. 129–176. <https://doi.org/10.1016/B978-0-12-420118-7.00004-4>
- Hummerich, R., Reischl, G., Ehrlichmann, W., Machulla, H.-J., Heinz, A., Schloss, P., 2004. DASB -in vitro binding characteristics on human recombinant monoamine transporters with regard to its potential as positron emission tomography (PET) tracer. *J. Neurochem.* 90, 1218–1226.
<https://doi.org/10.1111/j.1471-4159.2004.02585.x>
- Humphrey, W., Dalke, A., Schulten, K., 1996. VMD: visual molecular dynamics. *J. Mol. Graph.* 14, 33–38, 27–28.
- Indarte, M., Madura, J.D., Surratt, C.K., 2008. Dopamine transporter comparative molecular modeling and binding site prediction using the LeuT(Aa) leucine transporter as a template. *Proteins* 70, 1033–1046.
<https://doi.org/10.1002/prot.21598>
- Inyushin, M.U., Arencibia-Albite, F., de la Cruz, A., Vázquez-Torres, R., Colon, K., Sanabria, P., Jiménez-Rivera, C.A., 2013. New method to visualize neurons with DAT in slices of rat VTA using fluorescent substrate for DAT, ASP⁺. *J. Neurosci. Neuroengineering* 2, 98–103.
<https://doi.org/10.1166/jnsne.2013.1040>

- Irwin, J.J., Sterling, T., Mysinger, M.M., Bolstad, E.S., Coleman, R.G., 2012. ZINC: A Free Tool to Discover Chemistry for Biology. *J. Chem. Inf. Model.* 52, 1757–1768. <https://doi.org/10.1021/ci3001277>
- Juárez Olguín, H., Calderón Guzmán, D., Hernández García, E., Barragán Mejía, G., 2016. The Role of Dopamine and Its Dysfunction as a Consequence of Oxidative Stress. *Oxid. Med. Cell. Longev.* 2016, 1–13. <https://doi.org/10.1155/2016/9730467>
- Kador, P.F., Kinoshita, J.H., Sharpless, N.E., 1985. Aldose reductase inhibitors: a potential new class of agents for the pharmacological control of certain diabetic complications. *J. Med. Chem.* 28, 841–849.
- Kantcheva, A.K., Quick, M., Shi, L., Winther, A.-M.L., Stolzenberg, S., Weinstein, H., Javitch, J.A., Nissen, P., 2013. Chloride binding site of neurotransmitter sodium symporters. *Proc. Natl. Acad. Sci.* 110, 8489–8494. <https://doi.org/10.1073/pnas.1221279110>
- Kohut, S.J., Fivel, P.A., Blough, B.E., Rothman, R.B., Mello, N.K., 2013. Effects of methcathinone and 3-Cl-methcathinone (PAL-434) in cocaine discrimination or self-administration in rhesus monkeys. *Int. J. Neuropsychopharmacol.* 16, 1985–1998. <https://doi.org/10.1017/S146114571300059X>
- Koldsø, H., Autzen, H.E., Grouleff, J., Schiøtt, B., 2013. Ligand Induced Conformational Changes of the Human Serotonin Transporter Revealed by Molecular Dynamics Simulations. *PLOS ONE* 8, e63635. <https://doi.org/10.1371/journal.pone.0063635>
- Kristensen, A.S., Andersen, J., Jorgensen, T.N., Sorensen, L., Eriksen, J., Loland, C.J., Stromgaard, K., Gether, U., 2011. SLC6 Neurotransmitter Transporters: Structure, Function, and Regulation. *Pharmacol. Rev.* 63, 585–640. <https://doi.org/10.1124/pr.108.000869>
- Lau, T., Proissl, V., Ziegler, J., Schloss, P., 2015. Visualization of neurotransmitter uptake and release in serotonergic neurons. *J. Neurosci. Methods* 241, 10–17. <https://doi.org/10.1016/j.jneumeth.2014.12.009>
- Lomize, M.A., Lomize, A.L., Pogozheva, I.D., Mosberg, H.I., 2006. OPM: Orientations of Proteins in Membranes database. *Bioinformatics* 22, 623–625. <https://doi.org/10.1093/bioinformatics/btk023>
- López-Arnau, R., Martínez-Clemente, J., Pubill, D., Escubedo, E., Camarasa, J., 2012. Comparative neuropharmacology of three psychostimulant cathinone derivatives: butylone, mephedrone and methylone: Neuropharmacology of cathinone derivatives. *Br. J. Pharmacol.* 167, 407–420. <https://doi.org/10.1111/j.1476-5381.2012.01998.x>
- MacKerell, A.D., Bashford, D., Bellott, M., Dunbrack, R.L., Evanseck, J.D., Field, M.J., Fischer, S., Gao, J., Guo, H., Ha, S., Joseph-McCarthy, D., Kuchnir, L., Kuczera, K., Lau, F.T., Mattos, C., Michnick, S., Ngo, T., Nguyen, D.T., Prodhom, B., Reiher, W.E., Roux, B., Schlenkrich, M., Smith, J.C., Stote, R., Straub, J., Watanabe, M., Wiórkiewicz-Kuczera, J., Yin, D., Karplus, M., 1998. All-atom empirical potential for molecular modeling and dynamics studies of proteins. *J. Phys. Chem. B* 102, 3586–3616. <https://doi.org/10.1021/jp973084f>
- Madras, B.K., Xie, Z., Lin, Z., Jassen, A., Panas, H., Lynch, L., Johnson, R., Livni, E., Spencer, T.J., Bonab, A.A., Miller, G.M., Fischman, A.J., 2006. Modafinil Occupies Dopamine and Norepinephrine Transporters in Vivo and Modulates the Transporters and Trace Amine Activity in Vitro. *J. Pharmacol. Exp. Ther.* 319, 561–569. <https://doi.org/10.1124/jpet.106.106583>
- Martí, Y., Matthaeus, F., Lau, T., Schloss, P., 2017. Methyl-4-phenylpyridinium (MPP⁺) differentially affects monoamine release and re-uptake in murine embryonic stem cell-derived dopaminergic and serotonergic neurons. *Mol. Cell. Neurosci.* 83, 37–45. <https://doi.org/10.1016/j.mcn.2017.06.009>
- Martyna, G.J., Tobias, D.J., Klein, M.L., 1994. Constant pressure molecular dynamics algorithms. *J. Chem. Phys.* 101, 4177–4189. <https://doi.org/10.1063/1.467468>
- Matthaeus, F., Schloss, P., Lau, T., 2015. Differential Uptake Mechanisms of Fluorescent Substrates into Stem-Cell-Derived Serotonergic Neurons. *ACS Chem. Neurosci.* 6, 1906–1912. <https://doi.org/10.1021/acschemneuro.5b00219>
- Mavel, S., Mincheva, Z., Méheux, N., Carcenac, Y., Guilloteau, D., Abarbri, M., Emond, P., 2012. QSAR study and synthesis of new phenyltropanes as ligands of the dopamine transporter (DAT). *Bioorg. Med. Chem.* 20, 1388–1395. <https://doi.org/10.1016/j.bmc.2012.01.014>
- Milletti, F., Storch, L., Goracci, L., Bendels, S., Wagner, B., Kansy, M., Cruciani, G., 2010. Extending pKa prediction accuracy: High-throughput pKa measurements to understand pKa modulation of new chemical series. *Eur. J. Med. Chem.* 45, 4270–4279. <https://doi.org/10.1016/j.ejmech.2010.06.026>
- Moroy, G., Sperandio, O., Rielland, S., Khemka, S., Druart, K., Goyal, D., Perahia, D., Miteva, M.A., 2015. Sampling of conformational ensemble for virtual screening using molecular dynamics simulations and normal mode analysis. *Future Med. Chem.* 7, 2317–2331. <https://doi.org/10.4155/fmc.15.150>

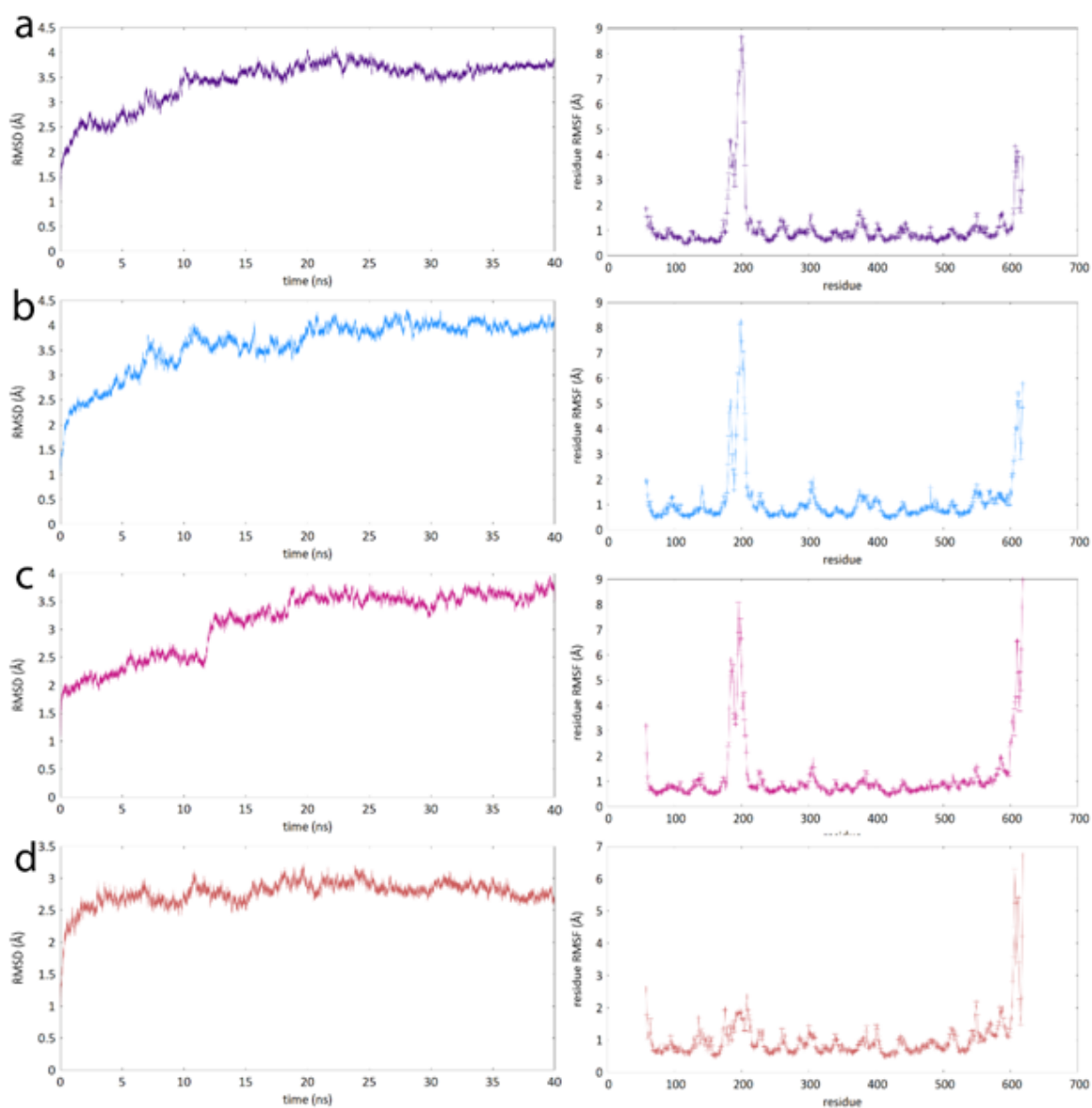
- Morris, G.M., Huey, R., Lindstrom, W., Sanner, M.F., Belew, R.K., Goodsell, D.S., Olson, A.J., 2009. AutoDock4 and AutoDockTools4: Automated docking with selective receptor flexibility. *J. Comput. Chem.* 30, 2785–2791. <https://doi.org/10.1002/jcc.21256>
- Mysinger, M.M., Carchia, M., Irwin, J.J., Shoichet, B.K., 2012. Directory of Useful Decoys, Enhanced (DUD-E): Better Ligands and Decoys for Better Benchmarking. *J. Med. Chem.* 55, 6582–6594. <https://doi.org/10.1021/jm300687e>
- Oz, M., Libby, T., Kivell, B., Jaligam, V., Ramamoorthy, S., Shippenberg, T.S., 2010. Real-time, spatially resolved analysis of serotonin transporter activity and regulation using the fluorescent substrate, ASP+. *J. Neurochem.* 114, 1019–1029. <https://doi.org/10.1111/j.1471-4159.2010.06828.x>
- Pavlin, M., Repič, M., Vianello, R., Mavri, J., 2016. The Chemistry of Neurodegeneration: Kinetic Data and Their Implications. *Mol. Neurobiol.* 53, 3400–3415. <https://doi.org/10.1007/s12035-015-9284-1>
- Penmatsa, A., Wang, K.H., Gouaux, E., 2013. X-ray structure of dopamine transporter elucidates antidepressant mechanism. *Nature* 503, 85–90. <https://doi.org/10.1038/nature12533>
- Phillips, J.C., Braun, R., Wang, W., Gumbart, J., Tajkhorshid, E., Villa, E., Chipot, C., Skeel, R.D., Kalé, L., Schulten, K., 2005. Scalable molecular dynamics with NAMD. *J. Comput. Chem.* 26, 1781–1802. <https://doi.org/10.1002/jcc.20289>
- Ravna, A.W., Jaroczyk, M., Sylte, I., 2006. A homology model of SERT based on the LeuT(Aa) template. *Bioorg. Med. Chem. Lett.* 16, 5594–5597. <https://doi.org/10.1016/j.bmcl.2006.08.028>
- Reith, M.E.A., Blough, B.E., Hong, W.C., Jones, K.T., Schmitt, K.C., Baumann, M.H., Partilla, J.S., Rothman, R.B., Katz, J.L., 2015. Behavioral, biological, and chemical perspectives on atypical agents targeting the dopamine transporter. *Drug Alcohol Depend.* 147, 1–19. <https://doi.org/10.1016/j.drugalcdep.2014.12.005>
- Robertson, S.D., Matthies, H.J.G., Galli, A., 2009. A Closer Look at Amphetamine-Induced Reverse Transport and Trafficking of the Dopamine and Norepinephrine Transporters. *Mol. Neurobiol.* 39, 73–80. <https://doi.org/10.1007/s12035-009-8053-4>
- Rothman, R.B., 2003. (+)-Fenfluramine and Its Major Metabolite, (+)-Norfenfluramine, Are Potent Substrates for Norepinephrine Transporters. *J. Pharmacol. Exp. Ther.* 305, 1191–1199. <https://doi.org/10.1124/jpet.103.049684>
- Schloss, P., Matthäus, F., Lau, T., 2015. Shine bright: considerations on the use of fluorescent substrates in living monoaminergic neurons in vitro. *Neural Regen. Res.* 10, 1383.
- Schmitt, K.C., Rothman, R.B., Reith, M.E.A., 2013. Nonclassical Pharmacology of the Dopamine Transporter: Atypical Inhibitors, Allosteric Modulators, and Partial Substrates. *J. Pharmacol. Exp. Ther.* 346, 2–10. <https://doi.org/10.1124/jpet.111.191056>
- Schwartz, J.W., Blakely, R.D., DeFelice, L.J., 2003. Binding and Transport in Norepinephrine Transporters REAL-TIME, SPATIALLY RESOLVED ANALYSIS IN SINGLE CELLS USING A FLUORESCENT SUBSTRATE. *J. Biol. Chem.* 278, 9768–9777. <https://doi.org/10.1074/jbc.M209824200>
- Seddik, A., Holy, M., Weissensteiner, R., Zdrzil, B., Sitte, H.H., Ecker, G.F., 2013. Probing the Selectivity of Monoamine Transporter Substrates by Means of Molecular Modeling. *Mol. Inform.* 32, 409–413. <https://doi.org/10.1002/minf.201300013>
- Sinko, W., de Oliveira, C., Williams, S., Van Wynsberghe, A., Durrant, J.D., Cao, R., Oldfield, E., McCammon, J.A., 2011. Applying Molecular Dynamics Simulations to Identify Rarely Sampled Ligand-bound Conformational States of Undecaprenyl Pyrophosphate Synthase, an Antibacterial Target: Identifying Rare States of UPPS. *Chem. Biol. Drug Des.* 77, 412–420. <https://doi.org/10.1111/j.1747-0285.2011.01101.x>
- Spyrakakis, F., Benedetti, P., Decherchi, S., Rocchia, W., Cavalli, A., Alcaro, S., Ortuso, F., Baroni, M., Cruciani, G., 2015. A Pipeline To Enhance Ligand Virtual Screening: Integrating Molecular Dynamics and Fingerprints for Ligand and Proteins. *J. Chem. Inf. Model.* 55, 2256–2274. <https://doi.org/10.1021/acs.jcim.5b00169>
- Spyrakakis, F., Cavasotto, C.N., 2015. Open challenges in structure-based virtual screening: Receptor modeling, target flexibility consideration and active site water molecules description. *Arch. Biochem. Biophys.* 583, 105–119. <https://doi.org/10.1016/j.abb.2015.08.002>
- Spyrakakis, F., Cellini, B., Bruno, S., Benedetti, P., Carosati, E., Cruciani, G., Micheli, F., Felici, A., Cozzini, P., Kellogg, G.E., Voltattorni, C.B., Mozzarelli, A., 2014. Targeting cystalysin, a virulence factor of treponema denticola-supported periodontitis. *ChemMedChem* 9, 1501–1511. <https://doi.org/10.1002/cmdc.201300527>

- Spyrakakis, F., Felici, P., Bayden, A.S., Salsi, E., Miggiano, R., Kellogg, G.E., Cozzini, P., Cook, P.F., Mozzarelli, A., Campanini, B., 2013a. Fine tuning of the active site modulates specificity in the interaction of O-acetylserine sulfhydrylase isozymes with serine acetyltransferase. *Biochim. Biophys. Acta BBA - Proteins Proteomics* 1834, 169–181. <https://doi.org/10.1016/j.bbapap.2012.09.009>
- Spyrakakis, F., Singh, R., Cozzini, P., Campanini, B., Salsi, E., Felici, P., Raboni, S., Benedetti, P., Cruciani, G., Kellogg, G.E., Cook, P.F., Mozzarelli, A., 2013b. Isozyme-Specific Ligands for O-acetylserine sulfhydrylase, a Novel Antibiotic Target. *PLoS ONE* 8, e77558. <https://doi.org/10.1371/journal.pone.0077558>
- Tavoulari, S., Margheritis, E., Nagarajan, A., DeWitt, D.C., Zhang, Y.-W., Rosado, E., Ravera, S., Rhoades, E., Forrest, L.R., Rudnick, G., 2016. Two Na⁺ Sites Control Conformational Change in a Neurotransmitter Transporter Homolog. *J. Biol. Chem.* 291, 1456–1471. <https://doi.org/10.1074/jbc.M115.692012>
- Totrov, M., Abagyan, R., 2008. Flexible ligand docking to multiple receptor conformations: a practical alternative. *Curr. Opin. Struct. Biol.* 18, 178–184. <https://doi.org/10.1016/j.sbi.2008.01.004>
- Underwood J., Cross S., 2009. *General and Systematic Pathology - 5th Edition*, 5th Edition. ed. Churchill Livingstone 2009.
- Vanommeslaeghe, K., Hatcher, E., Acharya, C., Kundu, S., Zhong, S., Shim, J., Darian, E., Guvench, O., Lopes, P., Vorobyov, I., Mackerell, A.D., 2009. CHARMM general force field: A force field for drug-like molecules compatible with the CHARMM all-atom additive biological force fields. *J. Comput. Chem.* NA-NA. <https://doi.org/10.1002/jcc.21367>
- Wang, K.H., Penmatsa, A., Gouaux, E., 2015. Neurotransmitter and psychostimulant recognition by the dopamine transporter. *Nature* 521, 322–327. <https://doi.org/10.1038/nature14431>
- Webb, B., Sali, A., 2016. Comparative Protein Structure Modeling Using MODELLER. *Curr. Protoc. Bioinforma.* 54, 5.6.1-5.6.37. <https://doi.org/10.1002/cpbi.3>
- Wiemerslage, L., Schultz, B.J., Ganguly, A., Lee, D., 2013. Selective degeneration of dopaminergic neurons by MPP⁺ and its rescue by D2 autoreceptors in *Drosophila* primary culture. *J. Neurochem.* 126, 529–540. <https://doi.org/10.1111/jnc.12228>
- Wimalasena, D.S., Perera, R.P., Heyen, B.J., Balasooriya, I.S., Wimalasena, K., 2008. Vesicular Monoamine Transporter Substrate/Inhibitor Activity of MPTP/MPP⁺ Derivatives: A Structure–Activity Study. *J. Med. Chem.* 51, 760–768. <https://doi.org/10.1021/jm070875p>
- Yamashita, A., Singh, S.K., Kawate, T., Jin, Y., Gouaux, E., 2005. Crystal structure of a bacterial homologue of Na⁺/Cl⁻-dependent neurotransmitter transporters. *Nature* 437, 215–223. <https://doi.org/10.1038/nature03978>
- Yu, W., He, X., Vanommeslaeghe, K., MacKerell, A.D., 2012. Extension of the CHARMM General Force Field to sulfonyl-containing compounds and its utility in biomolecular simulations. *J. Comput. Chem.* 33, 2451–2468. <https://doi.org/10.1002/jcc.23067>
- Zapata, A., Kivell, B., Han, Y., Javitch, J.A., Bolan, E.A., Kuraguntla, D., Jaligam, V., Oz, M., Jayanthi, L.D., Samuvel, D.J., Ramamoorthy, S., Shippenberg, T.S., 2007. Regulation of dopamine transporter function and cell surface expression by D3 dopamine receptors. *J. Biol. Chem.* 282, 35842–35854. <https://doi.org/10.1074/jbc.M611758200>

Human Dopamine Transporter: The first implementation of a combined *in silico/in vitro*-approach revealing the substrate and inhibitor specificities

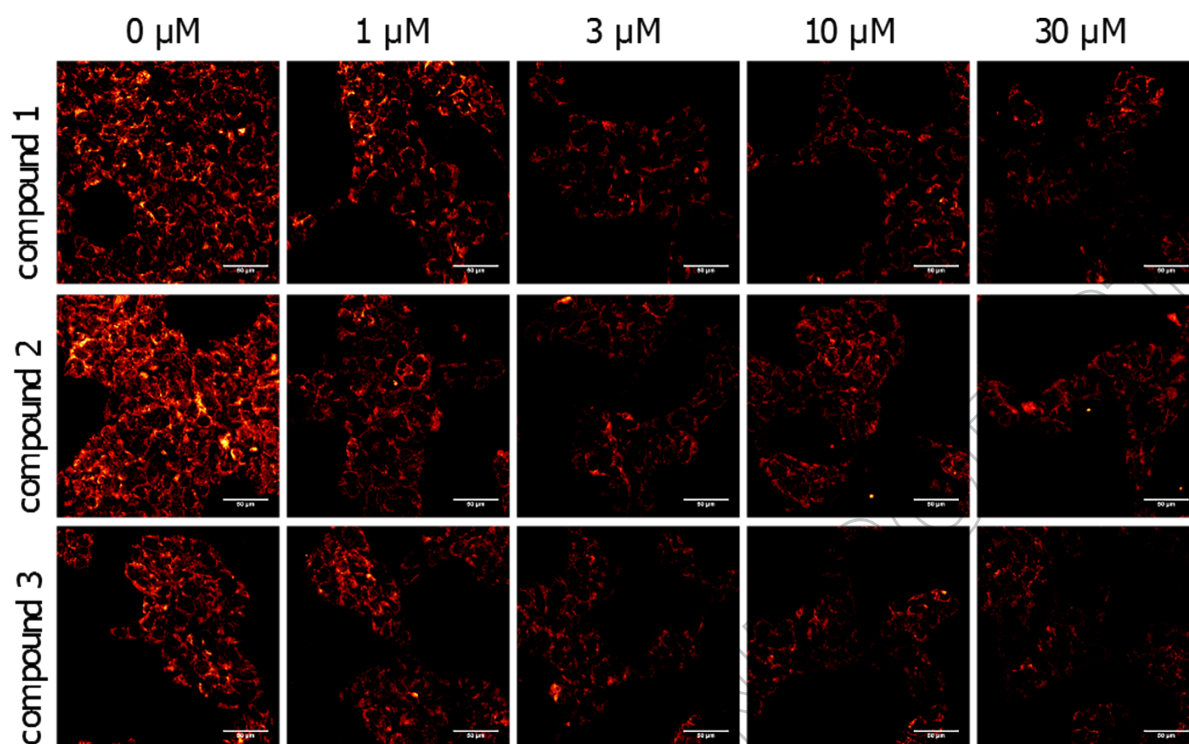
Teodora Djikic¹, Yasmina Marti^{2,6}, Francesca Spyrakis³, Thorsten Lau², Paolo Benedetti⁴, Gavin Davey⁵, Patrick Schloss⁶ and Kemal Yelekci¹

1. Department of Bioinformatics and Genetics, Kadir Has University, Cibali campus, Fatih, 34083, Istanbul, Turkey
2. Hector Institute for Translational Brain Research, Central Institute of Mental Health, Medical Faculty Mannheim, Heidelberg University, Germany
3. Department of Drug Science and Technology, University of Turin, via P. Giuria 9, 10125 Turin, Italy
4. Department of Chemistry, Biology and Biotechnology, University of Perugia, via Elce di sotto 8, 06123 Perugia, Italy
5. School of Biochemistry and Immunology, Trinity College Dublin, Dublin 2, Ireland
6. Biochemical Laboratory, Psychiatry and Psychotherapy Department, Central Institute of Mental Health, Medical Faculty Mannheim, Heidelberg University, Germany



Supporting Information S1: RMSD and residue RMSF values after 40 ns MD simulation.

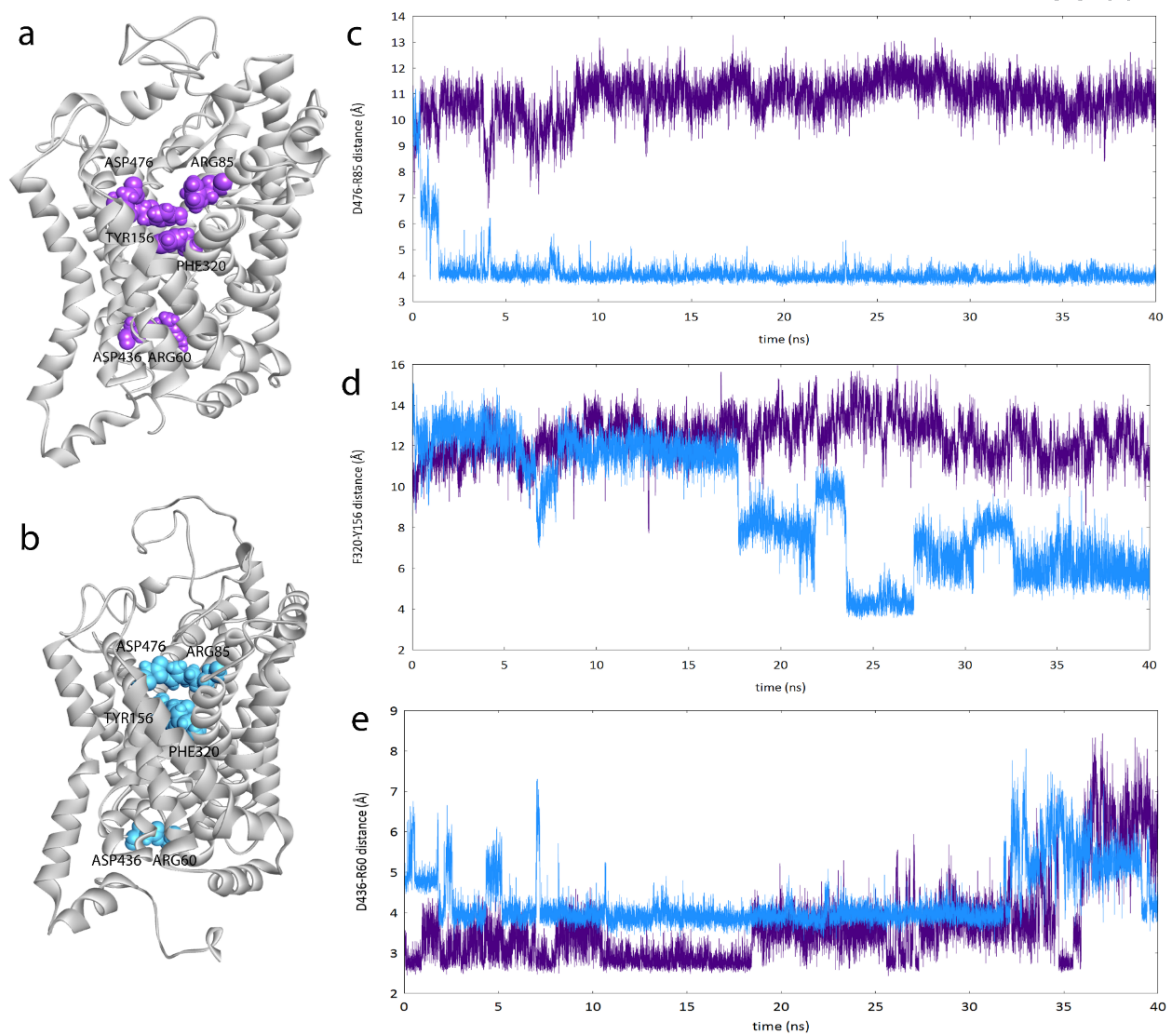
RMSD (right) and residue RMSF values (left) of hDAT empty transporter in purple (a), hDAT-amphetamine – blue (b), hDAT-cocaine - pink (c) and hDAT-modafinil – orange (d) complexes. The RMSD stabilized around 4 Å (for all the simulations) from the reference conformation after approximately 5000 time steps (10 ns). From the RMSF measurement we reasonably observed that the most flexible residues were located in the extracellular loops.



Supporting Information S2: Alteration/inhibition of ASP+ uptake into HEK-hDAT cells.

HEK-hDAT were treated for 10 min with different concentrations (1 μM , 3 μM , 10 μM and 30 μM) of compounds **1**, **2** or **3**. Representative fluorescent images of HEK-hDAT with 30 s incubation of 10 μM ASP+ before and after incubation with the compounds.

ACCEPTED MANUSCRIPT



Supporting Information S3: Behaviour of amino acids of DATs gates over time in apo hDAT (purple) and hDAT-amphetamine complex (blue). (a) outward-open conformation: both extracellular gates are open and intracellular gate is closed (b) closed conformation: all the gates are closed. Distances between Asp476 and Arg85 that are forming outer extracellular gate(c), Phe320 and Tyr156 that are closing inner extracellular gate (d), distances between Asp436 and Arg60 that are opening the intracellular gate (e).